Title

Identification and characterization of functional homologs of nitrogenase cofactor biosynthesis protein NifB from methanogens

Journal

Proceedings of the National Academy of Sciences of the United States of America, 112(48)

ISSN

0027-8424

Authors

Fay, Aaron W
Wiig, Jared A
Lee, Chi Chung
et al.

Publication Date

2015-12-01

DOI

10.1073/pnas.1510409112

Identification and characterization of functional homologs of nitrogenase cofactor biosynthesis protein NifB from methanogens

Aaron W. Fay, Jared A. Wiig, Chi Chung Lee, and Yilin Hu[1]

Department of Molecular Biology and Biochemistry, University of California, Irvine, CA 92697-3900

Edited by Douglas C. Rees, Howard Hughes Medical Institute, Caltech, Pasadena, CA, and approved October 27, 2015 (received for review May 27, 2015)

Nitrogenase biosynthesis protein NifB catalyzes the radical *S*-adenosyl-L-methionine (SAM)-dependent insertion of carbide into the M cluster, the cofactor of the molybdenum nitrogenase from *Azotobacter vinelandii*. Here, we report the identification and characterization of two naturally "truncated" homologs of NifB from *Methanosarcina acetivorans* (NifB^{Ma}) and *Methanobacterium thermoautotrophicum* (NifB^{Mt}), which contain a SAM-binding domain at the N terminus but lack a domain toward the C terminus that shares homology with NifX, an accessory protein in M cluster biosynthesis. NifB^{Ma} and NifB^{Mt} are monomeric proteins containing a SAM-binding [Fe_4S_4] cluster (designated the SAM cluster) and a [Fe_4S_4]-like cluster pair (designated the K cluster) that can be processed into an [Fe_8S_9] precursor to the M cluster (designated the L cluster). Further, the K clusters in NifB^{Ma} and NifB^{Mt} can be converted to L clusters upon addition of SAM, which corresponds to their ability to heterologously donate L clusters to the biosynthetic machinery of *A. vinelandii* for further maturation into the M clusters. Perhaps even more excitingly, NifB^{Ma} and NifB^{Mt} can catalyze the removal of methyl group from SAM and the abstraction of hydrogen from this methyl group by 5′-deoxyadenosyl radical that initiates the radical-based incorporation of methyl-derived carbide into the M cluster. The successful identification of NifB^{Ma} and NifB^{Mt} as functional homologs of NifB not only enabled classification of a new subset of radical SAM methyltransferases that specialize in complex metallocluster assembly, but also provided a new tool for further characterization of the distinctive, NifB-catalyzed methyl transfer and conversion to an iron-bound carbide.

nitrogenase | NifB | methanogens | radical SAM | homologs

Nitrogenase biosynthesis protein NifB is a radical *S*-adenosyl-L-methionine (SAM) enzyme that plays an essential role in the biosynthesis of the M cluster, a [$MoFe_8S_9C$-homocitrate] cluster that serves as the cofactor of the molybdenum (Mo) nitrogenase from *Azotobacter vinelandii* (1–7). Carrying a signature CxxxCxxC motif at its N terminus that houses the SAM-binding [Fe_4S_4] cluster (designated the SAM cluster), NifB also contains a number of additional ligands that could accommodate coordination of the entire complement of iron (Fe) atoms of the M cluster (Fig. S1). Moreover, it shares sequence homology with NifX, an accessory protein in M-cluster biosynthesis (8), toward its C terminus (Fig. S1). Characterization of the NifB protein from *A. vinelandii* had long been hampered by the instability of NifB in aqueous solutions until this protein was expressed as part of a NifEN-B fusion protein, wherein NifB was fused with and protected by NifEN, the biosynthetic apparatus immediately downstream of NifB along the M-cluster assembly pathway (9). Expression of the NifEN-B fusion protein in *A. vinelendii* was "modeled" after a naturally occurring NifEN-B fusion protein in *Clostridium pasteurianum*, which has the N terminus of NifB fused with the C terminus of NifN at a 1:1 molar ratio.

Subsequent studies of NifEN-B have demonstrated that, in the presence of SAM, NifB is capable of inserting a carbide concomitant with the coupling of a [Fe_4S_4]-like cluster pair (designated the K cluster) into an [Fe_8S_9C] cluster (designated the L cluster), which represents an all-iron core of the M cluster (9, 10). More excitingly, these studies have established the methyl group of SAM as the source of carbide, which is presumably transferred from SAM to the K cluster on NifB and processed initially by a hydrogen abstraction step that is enabled by a SAM-derived 5′-deoxyadenosyl radical (5′-dA•) (Fig. S2). The resultant methylene radical is further deprotonated into a carbide ion (C^{4-}) concomitant with the radical-based rearrangement and coupling of the two [Fe_4S_4]-like modules of the K cluster into an [Fe_8S_9C] L cluster (Fig. S2) (11). The L cluster can then be converted into a mature M cluster on NifEN upon insertion of Mo and homocitrate by NifH (the reductase component of Mo ntirogenase), followed by delivery of the M cluster from NifEN to its target location in NifDK (the catalytic component of Mo nitrogenase) via direct protein–protein interactions (Fig. S2) (12–16).

Despite the success in characterizing the *A. vinelandii* NifB protein (designated NifB^{Av}) in the form of NifEN-B fusion protein, the presence of NifEN entity in this protein has precluded an independent analysis of the subunit and cluster compositions of NifB^{Av}. Moreover, the impact of the "NifX domain" on the functionality of NifB^{Av} has not been evaluated to date. Interestingly, two naturally "truncated" NifB homologs, which do not have the "NifX domain" toward the C termini of their sequences, can be identified in two methanogenic, nitrogen-fixing organisms: one of them (designated NifB^{Ma}) is from the mesophilic organism, *Methanosarcina acetivorans* (17); whereas the other (designated NifB^{Mt}) is from the thermophilic organism, *Methanobacterium thermoautotrophicum* (also named *Methanobacter*

Significance

Nitrogenase biosynthesis protein NifB catalyzes the radical *S*-adenosyl-L-methionine (SAM)-dependent insertion of carbide into the nitrogenase cofactor, M cluster, in a chemically unprecedented and biologically important reaction. The observation that two naturally "truncated" NifB homologs from *Methanosarcina acetivorans* (NifB^{Ma}) and *Methanobacterium thermoautotrophicum* (NifB^{Mt}) are functional equivalents of NifB from the diazotrophic organism, *Azotobacter vinelandii*, establishes the minimum sequence requirement for a functional NifB protein and reveals the species-dependent difference between members of this protein family; more importantly, it leads to the categorization of a distinct class of radical SAM methyltransferases that function in complex metallocluster assembly while opening up new avenues to study the structure and mechanism of NifB.

Author contributions: Y.H. designed research; A.W.F., J.A.W., and C.C.L. performed research; A.W.F., J.A.W., C.C.L., and Y.H. analyzed data; and Y.H. wrote the paper.

The authors declare no conflict of interest.

This article is a PNAS Direct Submission.

[1]To whom correspondence should be addressed. Email: yilinh@uci.edu.

This article contains supporting information online at www.pnas.org/lookup/suppl/doi:10.1073/pnas.1510409112/-/DCSupplemental.

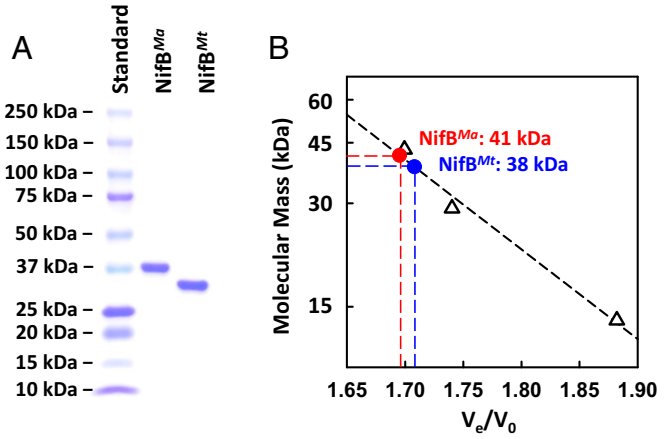

Fig. 1. Molecular masses of NifB^{Ma} and NifB^{Mt}. (*A*) Coomassie blue-stained 4–15% SDS/PAGE (BioRad Mini-PROTEAN TGX SDS/PAGE) of NifB^{Ma} and NifB^{Mt}. Lanes from left to right: 10 μL of protein standards (BioRad Precision Plus Protein Kaleidoscope Standards), 2 μg of purified NifB^{Ma}, and 2 μg of purified NifB^{Mt}. (*B*) Determination of the native molecular masses of NifB^{Ma} and NifB^{Mt} by gel filtration. V_0, void volume; V_e, elution volume. Protein standards (GE Healthcare Biosciences), shown in open triangles, are: ribonuclease A (13.7 kDa), carbonic anhydrase (29 kDa), and ovalbumin (43 kDa).

thermoautotrophicus) (18). These NifB homologs were identified from the genomes of *M. acetivorans* C2A strain (Gene ID 638179084; Gene Symbol MA4195) and *M. thermoautotrophicum* Delta H strain (Gene ID 638156427; Gene Symbol MTH1871) at the website of Integrated Microbial Genomes (https://img.jgi.doe.gov/cgi-bin/w/main.cgi).

Whereas shorter in length, NifB^{Ma} and NifB^{Mt} share 69% and 64% sequence homology, respectively, with NifB^{Av} (Fig. S1). More importantly, like NifB^{Av}, they both contain the CxxxCxxC motif for coordination of the SAM cluster, as well as a number of conserved Cys and His residues for accommodation of an FeS precursor to the nitrogenase cofactor (Fig. S1). Such a simplified, NifX domain-free composition of NifB^{Ma} and NifB^{Mt} is appealing, as it not only enables assessment of the minimum sequence requirement for a functional NifB protein, but also facilitates heterologous expression of a stable form of NifB on its own, a feat that has not yet been accomplished in the case of NifB^{Av} due to the presence of "extra" hydrophobic stretches of polypeptides in the primary sequence of this protein.

Indeed, His-tagged NifB^{Ma} and NifB^{Mt} were successfully coexpressed with the FeS assembly machinery, IscSUA, in *Escherichia coli* strain BL21(DE3) and purified at ~350 and ~180 mg/g wet cells, respectively, as intact, soluble proteins. The molecular masses of the subunits of NifB^{Ma} and NifB^{Mt} were confirmed as 38 kDa and 35 kDa, respectively, by SDS/PAGE analysis (Fig. 1*A*), whereas the apparent native molecular masses of NifB^{Ma} and NifB^{Mt} were determined as 41 kDa and 38 kDa, respectively, by gel filtration chromatography (Fig. 1*B*). These observations suggest a monomeric composition of both NifB^{Ma} and NifB^{Mt}, which correlate further with the 1:1 molar ratio between the NifEN and NifB entities in the NifEN-B fusion protein, a ratio that implies the action of NifB as a monomer by interacting in a one-on-one manner with the two αβ-dimers of NifEN (9). The in vitro reconstitution of NifB^{Ma} and NifB^{Mt} by $FeCl_3$ and Na_2S, followed by removal of excess Fe/S aggregates, resulted in a metal content of 14.0 ± 2.8 and 13.0 ± 2.2 mol Fe/mol protein, respectively, of NifB^{Ma} and NifB^{Mt}. Such an iron content would be consistent with the presence of three [Fe_4S_4] clusters in NifB^{Ma} or NifB^{Mt}, which could be assigned to one 4Fe SAM cluster and two 4Fe modules of the K cluster (Fig. S2). More importantly, it suggests that NifB^{Ma} and NifB^{Mt} contain all cluster species that are required to facilitate the K- to L-cluster conversion in the presence of SAM.

Consistent with this suggestion, high performance liquid chromatography (HPLC) analysis revealed that, like NifEN-B (Fig. 2, trace 3), NifB^{Ma} (Fig. 2, trace 4) or NifB^{Mt} (Fig. 2, trace 5) was capable of cleaving SAM into *S*-adenosyl-L-homocysteine (SAH) and 5′-deoxyadenosine (5′-dAH) in the presence of a reductant, dithionite. The observation of identical SAM cleavage products implies that NifB^{Ma} and NifB^{Mt} follow the same mechanism as that proposed for NifB^{Av} in catalyzing the SAM-dependent reaction, mobilizing the methyl group of one equivalent of SAM and subsequently abstracting a hydrogen atom from this methyl group by a 5′-dA• radical that is derived from a second equivalent of SAM (Fig. S2). Moreover, formation of the same reaction byproducts by NifB proteins as those by radical SAM RNA methyltransferases RlmN and Cfr (19, 20) points to a similarity between NifB and these two well-characterized members of a larger subset of radical SAM enzymes that catalyze methylation reactions using SAM or other methyl donor molecules as cosubstrates (see *Discussion*). Interestingly, NifB^{Ma} and NifB^{Mt} appeared to be more efficient than NifB^{Av} in cleaving SAM into SAH and 5′-dAH, as a substantial amount of SAM was left uncleaved when it was incubated with NifEN-B (Fig. 2, trace 3), but very little or almost no SAM was left uncleaved when it was incubated with NifB^{Ma} (Fig. 2, trace 4) or NifB^{Mt} (Fig. 2, trace 5) at an equimolar amount to that of NifB^{Av} (in NifEN-B). Moreover, unlike NifB^{Av} (in NifEN-B), which generated SAH and 5′-dAH at an approximate molar ratio of 1:1 (Fig. 2, trace 3), NifB^{Ma} or NifB^{Mt} generated much more SAH than 5′-dAH (Fig. 2, traces 4 and 5). The "asymmetric" formation of SAM cleavage products suggests that, compared with NifB^{Av}, NifB^{Ma} and NifB^{Mt} catalyze the removal of methyl group from SAM at a much faster rate than the formation of 5′-dAH that results from hydrogen abstraction by

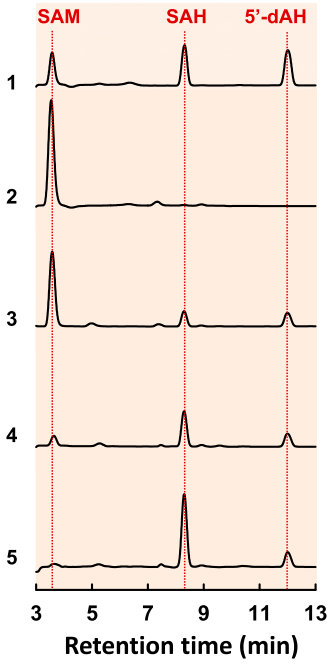

Fig. 2. SAM cleavage by NifB^{Ma} and NifB^{Mt}. HPLC elution profiles of (1) SAM, SAH, and 5′-dAH standards, (2) SAM alone, (3) SAM plus NifEN-B, (4) SAM plus NifB^{Ma}, and (5) SAM plus NifB^{Mt}. All samples contained dithionite. SAH was formed in the amounts of 0.20, 0.46, and 0.96 nanomole, respectively, per nanomole of NifEN-B, NifB^{Ma}, and NifB^{Mt}, whereas 5′-dAH was formed in the amounts of 0.18, 0.17, and 0.18 nanomole, respectively, per nanomole of NifEN-B, NifB^{Ma}, and NifB^{Mt}.

SAM-derived 5′-dA• radical. This observation underlines certain species-dependent differences between different members of the NifB protein family.

The close resemblance between the two NifB proteins from methanogens and their more complex counterpart in *A. vinelandii* is not only illustrated by the same SAM cleavage products they generate, but also highlighted by a highly similar spectroscopic response of their associated clusters to SAM treatment. Like NifEN-B (Fig. 3*A*, trace 1), both NifB^{Ma} (Fig. 3*A*, trace 3) and NifB^{Mt} (Fig. 3*A*, trace 5) displayed $S = 1/2$ EPR signals in the dithionite-reduced state, although the signal of NifEN-B was more complex than those of NifB^{Ma} and NifB^{Mt} due to the presence of additional cluster species in the NifEN entity of the fusion protein. Upon addition of SAM, there was a reduction in signal intensity in the cases of both NifB^{Ma} (Fig. 3*A*, trace 4) and NifB^{Mt} (Fig. 3*A*, trace 6), the same response to that observed in the case of NifEN-B (Fig. 3*A*, trace 2), which was associated with the disappearance of the K-cluster–originated, $S = 1/2$ signal following cluster conversion in the presence of SAM (9). Subtraction of the spectrum of the SAM-treated sample from that of the untreated sample in the dithionite-reduced state resulted in difference spectra of NifB^{Ma} (Fig. 3*B*, trace 2) and NifB^{Mt} (Fig. 3*A*, trace 3) with close resemblance to the difference spectrum of NifEN-B (Fig. 3*A*, trace 1), all displaying a similar line shape with g values of ∼2.02, ∼1.93, and ∼1.92. The observation that these difference spectra are composite $S = 1/2$ signals is consistent with the nature of K cluster as paired $[Fe_4S_4]^{1+}$ clusters in the presence of dithionite (9). More excitingly, in the indigo disulfonate (IDS)-oxidized state, the untreated NifB^{Ma} (Fig. 3*C*, trace 4) and NifB^{Mt} (Fig. 3*C*, trace 6) were EPR silent, whereas the SAM-treated NifB^{Ma} (Fig. 3*C*, trace 3) and NifB^{Mt} (Fig. 3*C*, trace 5) displayed strong signals that are highly similar to each other. Subtraction of the spectrum of the SAM-treated sample from that of the untreated sample in the IDS-oxidized state resulted in difference spectra of NifB^{Ma} (Fig. 3*D*, trace 2) and NifB^{Mt} (Fig. 3*D*, trace 3) with close likeness to the difference spectrum of NifEN-B (Fig. 3*D*, trace 1), which centered at a g value of ∼1.93. The NifEN-B contains some L clusters that are "backed up" on its NifEN entity, as this fusion protein was expressed in a *nifHDK*-deletion background, which does not contain NifH (a protein factor required to mature the NifEN-bound L cluster into an M cluster) and NifDK (the terminal "acceptor" of M cluster from NifEN) (9). Upon incubation with SAM, more L clusters are generated on NifEN-B due to the conversion of K clusters to L clusters on the NifB entity of this protein (9). Such a signal has been previously determined as the signature EPR feature of the $[Fe_8S_9]$ L cluster (12, 13), and the appearance of this signal in the spectra of SAM-treated NifB^{Ma} and NifB^{Mt} strongly suggests a K- to L-cluster conversion in these two proteins upon addition of SAM.

Direct proof in this regard came from the observation that SAM-treated NifB^{Ma} or NifB^{Mt} was capable of serving as a heterologous L-cluster donor to the assembly machinery of *A. vinelandii* in an in vitro cluster maturation assay. In this assay, SAM-treated NifB^{Ma} or NifB^{Mt} was incubated with dithionite, ATP, molybdate, homocitrate, NifH^{Av}, apo NifEN^{Av}, and apo NifDK^{Av}, which permitted transfer of the L cluster from NifB^{Ma} or NifB^{Mt} to apo NifEN^{Av}, maturation of the L cluster into an M cluster on NifEN^{Av} via NifH^{Av}-mediated insertion of Mo and homocitrate, and transfer of the matured M cluster to apo NifDK^{Av} that resulted in an active, reconstituted form of holo NifDK^{Av}. Interestingly, the SAM-treated NifB^{Ma} was nearly as active as the solvent-extracted L cluster in this heterologous in vitro cluster maturation assay, whereas the SAM-treated NifB^{Mt} was ∼30% active compared with both NifB^{Ma} and the extracted L cluster (Fig. 4). Addition of NifX^{Av} did not elevate the activities of NifB^{Ma} and NifB^{Mt} in the in vitro cluster maturation assays (Fig. S3), providing additional evidence that the NifX(-like) protein/domain is not essential for the functionality of NifB. This result is also consistent with the observation that a NifEN-B fusion protein containing a truncation of the NifX domain in NifB (designated NifEN-B′) was fully functional in the M-cluster maturation assay compared with the NifEN-B protein containing a full-length NifB entity (Fig. S4). The lower activity of NifB^{Mt} is likely due to the fact that this thermophilic protein does not work as efficiently as its

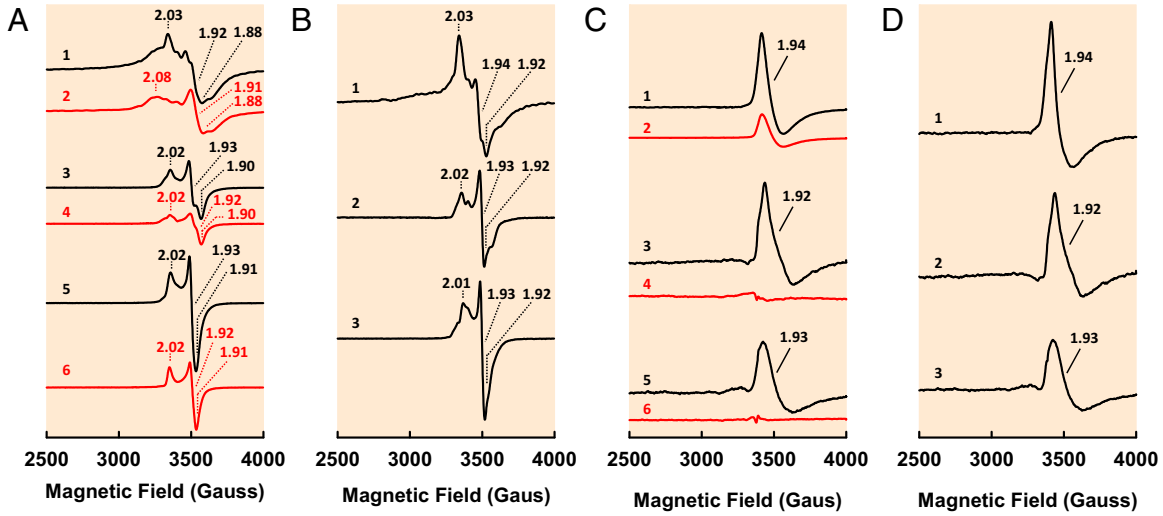

Fig. 3. EPR properties of NifB^{Ma} and NifB^{Mt}. (*A*) EPR spectra of dithionite-reduced (1) NifEN-B, (2) NifEN-B plus SAM, (3) NifB^{Ma}, (4) NifB^{Ma} plus SAM, (5) NifB^{Mt}, and (6) NifB^{Mt} plus SAM. Spectra were collected in perpendicular mode at 50 mW and 10 K. (*B*) Difference spectra between untreated and SAM-treated (1) NifEN-B, (2) NifB^{Ma}, and (3) NifB^{Mt} in the dithionite-reduced state. All difference spectra were derived from the corresponding spectra in *A* and multiplied by a factor of 1.5 for better visualization of features. (*C*) EPR spectra of IDS-oxidized (1) NifEN-B plus SAM, (2) NifEN-B, (3) NifB^{Ma} plus SAM, (4) NifB^{Ma}, (5) NifB^{Mt} plus SAM, and (6) NifB^{Mt}. The spectra of NifEN-B plus SAM (*C*, 1) and NifEN-B (*C*, 2) were multiplied by a factor of 0.5 for better adaptation to the size of the graph. The untreated NifEN-B contained some L clusters (*C*, 2) and, upon SAM treatment, more L clusters were generated in this protein (*C*, 1), as indicated by an increase in the magnitude of the L-cluster–specific, $g = 1.94$ signal. Spectra were collected in perpendicular mode at 50 mW and 15 K. (*D*) Difference spectra between untreated and SAM-treated (1) NifEN-B, (2) NifB^{Ma}, and (3) NifB^{Mt} in the IDS-oxidized state. All difference spectra were derived from the corresponding spectra in *C*, and the difference spectrum of NifEN-B (*D*, 1) was multiplied by a factor of 2. The g values are indicated.

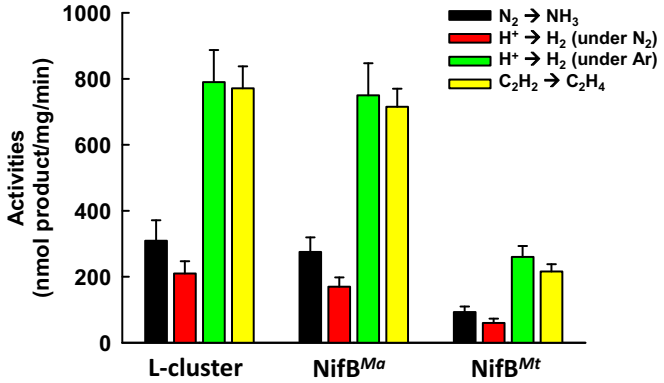

Fig. 4. Activities of $NifB^{Ma}$ and $NifB^{Mt}$ as L-cluster donors. Substrate-reducing activities of reconstituted NifDK in cluster maturation assays containing the extracted L cluster, $NifB^{Ma}$, and $NifB^{Mt}$ as the respective L-cluster donors along with dithionite, ATP, molydate, homocitrate, NifH, apo NifEN, and apo NifDK.

methophilic $NifB^{Ma}$ counterpart at the optimal assay temperature (30 °C), as well as a somewhat lower sequence homology between $NifB^{Av}$ and $NifB^{Mt}$ than that between $NifB^{Av}$ and $NifB^{Ma}$ (Fig. S1), which results in a less efficient transfer of the L cluster between $NifB^{Mt}$ and apo $NifEN^{Av}$ in the heterologous cluster maturation assay. Nevertheless, the results of these activity assays, together with those from the EPR analysis (see above), clearly demonstrate that the K- to L-cluster conversion is completed on NifB before the transfer of the L cluster to NifEN, a key sequence of events that could not be conclusively determined earlier through studies of the NifEN-B fusion protein. Moreover, the observation that the L cluster can be transferred from SAM-treated $NifB^{Ma}$ or $NifB^{Mt}$ to the assembly proteins of *A. vinelandii* points to the suitability to use this heterologous assay system to trace the fate of carbide from its origin (i.e., SAM), through the assembly intermediate (i.e., the L cluster), all of the way to the final cluster product (i.e., the M cluster).

The carbide-tracing experiments were performed by using [methyl-^{14}C] SAM as the initial carbon source. Consistent with the utilization of the SAM-derived methyl group for carbide insertion into the L cluster, the ^{14}C label appeared in both $NifB^{Ma}$ (Fig. 5*A*, 1) and $NifB^{Mt}$ (Fig. 5*B*, 1) upon incubation with [methyl-^{14}C] SAM. Following incubation with the heterologous cluster maturation components (see above) and reisolation of individual proteins from the incubation mixtures, however, the radiolabel disappeared from both NifB proteins (Fig. 5 *A* and *B*, 2) while appearing in the respective reconstituted $NifDK^{Av}$ proteins in these mixtures (Fig. 5 *A* and *B*, 3), suggesting that the ^{14}C-labeled L cluster on NifB was maturated into a ^{14}C-labeled M cluster and transferred to apo NifDK. In agreement with this suggestion, ^{14}C-labeled L and M clusters could be extracted from the NifB proteins (Fig. 5 *A* and *B*, 4, *Left*) and the reconstituted $NifDK^{Av}$ proteins (Fig. 5 *A* and *B*, 4, *Right*), respectively, and their identities were further confirmed by the activity of the former (i.e., the L cluster) in the cluster maturation assay and the latter (i.e., the M cluster) in the apo NifDK reconstitution assay. The L-cluster maturation assay contains dithionite, L cluster, apo NifEN, MgATP, molybdate, homocitrate, NifH, and apo NifDK, whereas the apo NifDK reconstitution assay contains dithionite, M cluster, and apo NifDK. Together, these results provide compelling evidence that that $NifB^{Ma}$ and $NifB^{Mt}$ follow the same radical SAM-dependent mechanism as that proposed for $NifB^{Av}$ to facilitate carbide insertion into the M-cluster of nitrogenase (Fig. S2).

It is interesting to note that, following cluster transfer, a small, background amount of radiolabel remained on $NifB^{Mt}$ (Fig. 5*B*, 2). This observation led to an important question of whether the residual radiolabel on $NifB^{Mt}$ originated from transfer of the ^{14}C-labeled methyl group to a certain protein residue as an intermediary step of carbide insertion, which would suggest a reaction pathway somewhat analogous to the one used by RlmN and Cfr to facilitate methylation of an inert C-H bond (19, 20). To address this question, $NifB^{Ma}$ and $NifB^{Mt}$ were prepared in the absence and presence of SAM and subsequently analyzed for posttranslational modification (PTM). As was observed in the case of $NifB^{Av}$ (11), no unique amino acid methylation events could be detected in SAM-treated $NifB^{Ma}$ and $NifB^{Mt}$ samples. This result suggests that methyltransfer by these NifB proteins does not route via a methylated amino acid intermediate; rather, it proceeds directly from SAM to the K cluster (Fig. S2). The residual radiolabel on $NifB^{Mt}$, therefore, was likely a result of inefficient transfer of radiolabeled cluster from the thermophilic $NifB^{Mt}$ to the mesophilic $NifEN^{Av}$ at a temperature (i.e., 25 °C) below that which was optimal for $NifB^{Mt}$. This argument is supported by the absence of radiolabel on the mesophilic $NifB^{Ma}$ following cluster transfer (Fig. 5*A*, 2), as well as the discrepancy between activities of $NifB^{Mt}$ and $NifB^{Ma}$ in the in vitro cluster maturation assays (Fig. 4).

Subsequent sequence analysis provided further explanation for the inability of NifB to generate a methylated amino acid intermediate, demonstrating that a pair of conserved Cys residues in the sequences of RlmN and Cfr, including one that serves as the site of intermediary methylation (Fig. S5*B*, blue arrow), are absent from the sequences of $NifB^{Av}$, $NifB^{Ma}$, and $NifB^{Mt}$. This feature sets the NifB proteins apart from the RlmN and Cfr proteins (Fig. S5*A*), which are emerging as a distinct class (class A) of a larger subset of radical SAM methyltransferases (RSMTs) that use conserved protein residues to facilitate methyltransfer (21, 22). The three NifB homologs are further distinguished from the other known classes of RSMTs (classes B–D), with classes B, C, and D carrying a cobalamin-binding domain, a HemN domain, and a methylenetetrahydrofolate domain, respectively, in addition to the canonical radical SAM domain (Fig. S5*A*). Excitingly, a BLAST search resulted in the identification of a large number of

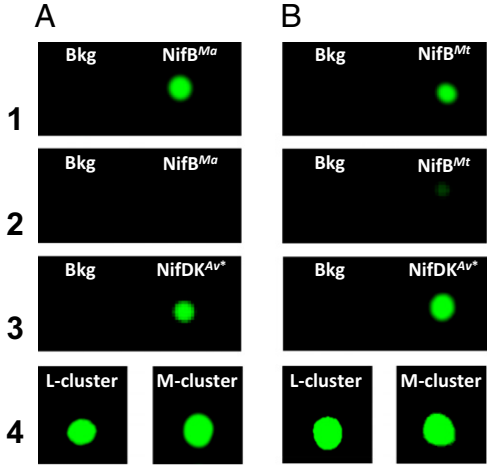

Fig. 5. Carbide insertion by $NifB^{Ma}$ and $NifB^{Mt}$. (1) His-tagged $NifB^{Ma}$ (*A*) or His-tagged $NifB^{Mt}$ (*B*) captured on affinity (IMAC) resin after incubation with [methyl-^{14}C] SAM. (2) His-tagged $NifB^{Ma}$ (*A*) or His-tagged $NifB^{Mt}$ (*B*) captured on affinity (IMAC) resin after incubation with [methyl-^{14}C] SAM, nontagged apo $NifEN^{Av}$, nontagged $NifH^{Av}$, and nontagged apo $NifDK^{Av}$. (3) Nontagged, reconstituted $NifDK^{Av}$ (designated $NifDK^{Av*}$) captured on anion-exchange (DEAE) resin after incubation with [methyl-^{14}C] SAM, His-tagged $NifB^{Ma}$ (*A*) or His-tagged $NifB^{Mt}$ (*B*), His-tagged apo $NifEN^{Av}$, and His-tagged $NifH^{Av}$. (4) Clusters extracted from the IMAC fraction in *A*, 1 and DEAC fraction in *A*, 3; and clusters extracted from the IMAC fraction in *B*, 1 and DEAE fraction in *B*, 3. Assays 2 and 3 also contained dithionite, ATP, molybdate, and homocitrate. Bkg, background.

proteins with high sequence homology to NifB^{Ma} and NifB^{Mt} (over 300 proteins with a homology of higher than 70% over a range of 85% of the sequence). The organisms expressing these truncated NifB homologs (60% methanogenic organisms and 40% non-methanogenic organisms) are widespread across the microbial biorealm; many of them are not nitrogen-fixing organisms, suggesting that the NifB proteins in these organisms carry out other functions that are yet to be identified. Sequence alignment of 45 closest matches of NifB homologs revealed the presence of the canonical radical SAM domain, as well as the same, conserved Cys and His residues as those identified in NifB^{Ma} and NifB^{Mt}, which potentially serve as FeS cluster-binding domains (Fig. S6). A new class of RSMTs (class E; Fig. S5*A* and Fig. S7) could be tentatively proposed based on this finding, which potentially specializes in radical SAM-based assembly of complex metallocenters.

Other than enabling the classification of a distinct subset of RSMTs, the successful identification of NifB^{Ma} or NifB^{Mt} as functional homologs of NifB^{Av} is exciting, as it opens up new avenues to study the structure and mechanism of the NifB protein, both of which remain relatively uncharacterized and promise to reveal completely unprecedented chemical reactions catalyzed by biological systems. The fact that both methanogen NifB homologs can be expressed alone in *E. coli* as soluble, intact proteins permits structural and biochemical analysis of NifB without interference of its protein partner and associated metal centers, a feat that has not been achieved so far through investigations of the NifEN-B fusion protein; moreover, it suggests the possibility to express a truncated version of NifB^{Av} in *E. coli*, which can then be used for comparative studies with its newly identified homologs in methanogens to shed light on the structure–function relationship of this important protein family. Novel mechanistic insights could be gained by studying these proteins side by side, and species-dependent differences revealed by these studies—such as a shift toward a higher SAH/5′-dAH ratio in the cases of NifB^{Ma} and NifB^{Mt}—could be explored to reveal differential mechanisms used by the NifB homologs to abstract hydrogen from the substrate-bound methyl group or identify additional functions of these proteins as methyltransferases in their native hosts. Additionally, important "snapshots" of carbide insertion pathway could be captured by mixing and matching the NifB protein from one organism with assembly components from another, which may back up certain intermediates on NifB due to a less efficient transfer of L clusters from NifB to its downstream assembly partner. All in all, the NifB homologs reported in this work provide a brand new tool in addition to the NifEN-B fusion protein (23) for further characterization of the distinctive methyl transfer and conversion to an iron-bound carbide by NifB, which is crucial for the unveiling of a chemically unique and biologically important reaction pathway.

Materials and Methods

Unless noted otherwise, all chemicals and reagents were obtained from Fisher Scientific or Sigma-Aldrich. Cell growth, protein purification, iron/sulfur reconstitution, molecular mass determination, iron determination, SAM cleavage assays, EPR analysis, cluster maturation assays, carbon-14 tracing experiments, cluster extraction, and PTM analysis were performed as described. See *SI Materials and Methods* for more information on these procedures.

Genes encoding the NifB homologs from *M. acetivorans* (NifB^{Ma}) and *M. thermoautotrophicum* (NifB^{Mt}) were codon optimized for *E. coli* expression and synthesized and cloned into the BamHI site of pET-3b and the NdeI site of pET-14b, respectively (GenScript USA). A short sequence encoding a 6xHis tag was inserted at the 5′-end of the gene encoding NifB^{Ma} before the cloning of this sequence into pET-3b, whereas the gene encoding NifB^{Mt} was placed behind a vector-derived sequence encoding a 6xHis tag when it was cloned into pET-14b. Each of these constructs was then cotransformed with a plasmid harboring *iscSUA* and *hscABfdx* genes—an ensemble of genes encoding Fe/S cluster assembly proteins (24–28)—into the *E. coli* strain BL21(DE3), resulting in strains overexpressing His-tagged forms of NifB^{Ma} (strain YM114EE) and NifB^{Mt} (strain YM127EE) upon induction by isopropyl β-D-1-thiogalactopyranoside (IPTG). The plasmid carrying *iscSUA* and *hscABfdx* genes was a generous gift from S. Leimkhüler (University of Potsdam, Potsdam, Germany). The gene encoding NifX from *A. vinelandii* (NifX^{Av}) was PCR amplified from the genomic DNA using a pair of primers (forward primer: 5′-ATGGTAGGTCTCAAATGTCCAGCCC GACCCGACAATTG-3′; reverse primer: 5′-ATGGTAGGTCTCAGCGCTTTCGTCCCAGCCTTCGGCGG-3′) and subsequently cloned into the BsaI site of pASK-IBA3 (IBA). This construct was transformed into the *E. coli* strain BL21-CodonPlus, resulting in a strain expressing a C terminus strep-tagged form of NifX^{Av} (strain YM300EE).

ACKNOWLEDGMENTS. We thank Prof. Markus Ribbe [University of California, Irvine (UCI)] for helpful discussion and technical support of biochemical experiments related to the NifEN-B′ fusion protein. This work was supported by UCI startup funds and a Hellman Fellowship (to Y.H.).

1. Burgess BK, Lowe DJ (1996) Mechanism of molybdenum nitrogenase. *Chem Rev* 96(7): 2983–3012.
2. Rees DC, et al. (2005) Structural basis of biological nitrogen fixation. *Philos Trans A Math Phys Eng Sci* 363(1829):971–984.
3. Ribbe MW, Hu Y, Hodgson KO, Hedman B (2014) Biosynthesis of nitrogenase metalloclusters. *Chem Rev* 114(8):4063–4080.
4. Frey PA, Hegeman AD, Ruzicka FJ (2008) The radical SAM superfamily. *Crit Rev Biochem Mol Biol* 43(1):63–88.
5. Broderick JB, Duffus BR, Duschene KS, Shepard EM (2014) Radical *S*-adenosylmethionine enzymes. *Chem Rev* 114(8):4229–4317.
6. Lancaster KM, et al. (2011) X-ray emission spectroscopy evidences a central carbon in the nitrogenase iron-molybdenum cofactor. *Science* 334(6058):974–977.
7. Spatzal T, et al. (2011) Evidence for interstitial carbon in nitrogenase FeMo cofactor. *Science* 334(6058):940.
8. Jacobson MR, et al. (1989) Physical and genetic map of the major *nif* gene cluster from *Azotobacter vinelandii*. *J Bacteriol* 171(2):1017–1027.
9. Wiig JA, Hu Y, Ribbe MW (2011) NifEN-B complex of *Azotobacter vinelandii* is fully functional in nitrogenase FeMo cofactor assembly. *Proc Natl Acad Sci USA* 108(21):8623–8627.
10. Lancaster KM, Hu Y, Bergmann U, Ribbe MW, DeBeer S (2013) X-ray spectroscopic observation of an interstitial carbide in NifEN-bound FeMoco precursor. *J Am Chem Soc* 135(2):610–612.
11. Wiig JA, Hu Y, Lee CC, Ribbe MW (2012) Radical SAM-dependent carbon insertion into the nitrogenase M-cluster. *Science* 337(6102):1672–1675.
12. Corbett MC, et al. (2006) Structural insights into a protein-bound iron-molybdenum cofactor precursor. *Proc Natl Acad Sci USA* 103(5):1238–1243.
13. Hu Y, Fay AW, Ribbe MW (2005) Identification of a nitrogenase FeMo cofactor precursor on NifEN complex. *Proc Natl Acad Sci USA* 102(9):3236–3241.
14. Hu Y, et al. (2006) FeMo cofactor maturation on NifEN. *Proc Natl Acad Sci USA* 103(46):17119–17124.
15. Hu Y, et al. (2006) Nitrogenase Fe protein: A molybdate/homocitrate insertase. *Proc Natl Acad Sci USA* 103(46):17125–17130.
16. Yoshizawa JM, et al. (2009) Optimization of FeMoco maturation on NifEN. *J Am Chem Soc* 131(26):9321–9325.
17. Oelgeschläger E, Rother M (2008) Carbon monoxide-dependent energy metabolism in anaerobic bacteria and archaea. *Arch Microbiol* 190(3):257–269.
18. Ferry JG (1999) Enzymology of one-carbon metabolism in methanogenic pathways. *FEMS Microbiol Rev* 23(1):13–38.
19. Grove TL, et al. (2011) A radically different mechanism for *S*-adenosylmethionine-dependent methyltransferases. *Science* 332(6029):604–607.
20. Boal AK, et al. (2011) Structural basis for methyl transfer by a radical SAM enzyme. *Science* 332(6033):1089–1092.
21. Zhang Q, van der Donk WA, Liu W (2012) Radical-mediated enzymatic methylation: a tale of two SAMS. *Acc Chem Res* 45(4):555–564.
22. Bauerle MR, Schwalm EL, Booker SJ (2015) Mechanistic diversity of radical *S*-adenosylmethionine (SAM)-dependent methylation. *J Biol Chem* 290(7):3995–4002.
23. Wiig JA, Hu Y, Ribbe MW (2015) Refining the pathway of carbide insertion into the nitrogenase M-cluster. *Nat Commun* 11(6):8034.
24. Frazzon J, Dean DR (2003) Formation of iron-sulfur clusters in bacteria: An emerging field in bioinorganic chemistry. *Curr Opin Chem Biol* 7(2):166–173.
25. Frazzon J, Fick JR, Dean DR (2002) Biosynthesis of iron-sulphur clusters is a complex and highly conserved process. *Biochem Soc Trans* 30(4):680–685.
26. Kriek M, Peters L, Takahashi Y, Roach PL (2003) Effect of iron-sulfur cluster assembly proteins on the expression of *Escherichia coli* lipoic acid synthase. *Protein Expr Purif* 28(2):241–245.
27. Cicchillo RM, et al. (2004) *Escherichia coli* lipoyl synthase binds two distinct [4Fe-4S] clusters per polypeptide. *Biochemistry* 43(37):11770–11781.
28. Lanz ND, et al. (2012) RlmN and AtsB as models for the overproduction and characterization of radical SAM proteins. *Methods Enzymol* 516:125–152.
29. Burgess BK (1990) The iron-molybdenum cofactor of nitrogenase. *Chem Rev* 90(8): 1377–1406.
30. Shah VK, Brill WJ (1977) Isolation of an iron-molybdenum cofactor from nitrogenase. *Proc Natl Acad Sci USA* 74(8):3249–3253.